Hindawi
Advances in Materials Science and Engineering
Volume 2018, Article ID 7026141, 11 pages
https://doi.org/10.1155/2018/7026141

Research Article

Core/Shell Structure of TiO_2-Coated MWCNTs for Thermal Protection for High-Temperature Processing of Metal Matrix Composites

Laura Angélica Ardila Rodriguez and Dilermando Nagle Travessa

Federal University of São Paulo (UNIFESP), Institute of Science and Technology, Laboratory of Advanced Metals and Processing, São José dos Campos, SP, Brazil

Correspondence should be addressed to Laura Angélica Ardila Rodriguez; laardilar88@gmail.com

Received 5 September 2017; Revised 3 November 2017; Accepted 21 November 2017; Published 11 January 2018

Academic Editor: Ilia Ivanov

The production of metal matrix composites with elevated mechanical properties depends largely on the reinforcing phase properties. Due to the poor oxidation resistance of multiwalled carbon nanotubes (MWCNTs) as well as their high reactivity with molten metal, the processing conditions for the production of MWCNT-reinforced metal matrix composites may be an obstacle to their successful use as reinforcement. Coating MWCNTs with a ceramic material that acts as a thermal protection would be an alternative to improve oxidation stability. In this work, MWCNTs previously functionalized were coated with titanium dioxide (TiO_2) layers of different thicknesses, producing a core-shell structure. Heat treatments at three different temperatures (500°C, 750°C, and 1000°C) were performed on coated nanotubes in order to form a stable metal oxide structure. The MWCNT/TiO_2 hybrids produced were evaluated in terms of thermal stability. Thermogravimetric analysis (TGA), X-ray diffraction (XRD), scanning electron microscopy (SEM), Fourier transform infrared spectroscopy (FTIR), Raman spectroscopy (RS), and X-ray photoelectron spectroscopy (XPS) were performed in order to investigate TiO_2-coated MWCNT structure and thermal stability under oxidative atmosphere. It was found that the thermal stability of the TiO_2-coated MWCNTs was dependent of the TiO_2 layer morphology that in turn depends on the heat treatment temperature.

1. Introduction

Since its discovery by Iijima in 1991 [1], carbon nanotubes (CNTs) have been very attractive for different applications due to their unique properties and structure. CNTs have been used as a reinforcement phase in several types of composite materials, including polymeric and ceramic matrix, and now are being used in high-performance metal matrix composites [2]. To take full advantage of CNTs as a reinforcement material, it is very important to preserve its structure as perfect as possible, during the composite processing. Furthermore, a good dispersion in the matrix and the formation of an interface that allows the load transfer between matrix and reinforcement are also important issues. It is well known that CNTs can support temperatures up to 2500°C in inert atmosphere, but in presence of oxygen, they can be completely decomposed at temperatures between 400 and 600°C, depending on their structure and purity level. In presence of metals like Al, it can form compounds like Al_4C_3 [3–5].

When processing metal matrix composites (MMCs), CNTs are commonly exposed to high temperatures and consequently preserving their integrity is a challenging task. Those processing routes include powder metallurgy [6–14], high-energy ball milling [15, 16], friction stir processing [17], spark plasma sintering [18], plasma spraying [19–21], and more recently laser sintering [22]. However, the obtained results are still not completely satisfactory, because the extreme processing conditions, either thermal or impact, can damage the CNT structure and cause a detrimental effect on the final mechanical properties of the composite. Bakshi et al. [23], for instance, reported that during plasma spraying

processing of Al/MWCNT composites, due to the interaction of the CNTs with the plasma plume, many defects were generated, which led to the formation of Al_4C_3 needles in contact with the aluminum matrix. Ci et al. [5] reported that this reaction for carbide formation usually occurs at amorphous regions of the nanotubes, at structural defects, or at the open sides of their extremities. Consequently, structural defects of CNTs are the precursors for the formation of nanoscale Al_4C_3 layers that are brittle and sensitive to moisture contact. Park and Lucas [24] found in a SiC_p/6061 Al composite that the interface formed by the reaction of SiC reinforcement and molten aluminum was Al_4C_3. The disintegration of Al_4C_3 occurred in less than 120 h when exposed to a wet environment, and failure during fracture toughness testing occurs predominately at the Al_4C_3 particle/matrix interface. For the above reasons, protecting CNTs during the MMC fabrication, without negatively affecting their integrity, is a prerequisite in order to keep their properties.

For severe processing conditions, such as high-power laser, used for synthesizing Inconel 718 super alloy reinforced by carbon nanotubes, Chen et al. [22] coated the CNT wall with NiP by electroless plating process, aiming to improve the CNTs to matrix adherence, preventing direct laser radiation and increasing the wettability. The authors reported a homogeneous dispersion of CNTs and a good interfacial bonding with the matrix. Jo et al. [25] coated carbon nanofibers with TiO_2 by the sol-gel method and dispersed it in aluminum matrix composites by the liquid pressing process, reporting that the coating not only protects the carbon nanofiber but also improves the mechanical properties of the composite.

In this context, the idea of creating a protection system for CNTs that will be subjected to high temperatures during the production of MMCs is promising. This procedure can guarantee a better structural stability and wettability with the matrix. It can even create an additional hardening effect in the composite, with the introduction of hard TiO_2 particles along with the CNTs.

The sol-gel technique is an ideal method to deposit layers in nanostructures and has been showed to be a feasible technique to coat CNTs without adverse effects in their intrinsic properties. In some works [26, 27], it has been reported successful TiO_2 coating on CNTs by the sol-gel processing route for photocatalysis and electrocatalysis applications. In these works, the obtained coating is amorphous and crystallizes at temperatures around 500°C. Eder and Windle [28] employed different metallic oxides to coat CNTs, obtaining crystalline coatings after calcinations at temperatures between 250°C and 400°C [29]. They found that Al_2O_3 was the best coating to avoid CNT oxidation. Similar result was found by Inam et al. [30] who obtained Al_2O_3-coated CNTs by atomic laser deposition.

In the present work, the thermal stability of TiO_2-coated MWCNTs, obtained by the sol-gel technique, was evaluated. This thermal stability was evaluated as a function of the coating layer thickness and for different coating structures, obtained from different calcination temperatures. Fourier transform infrared spectroscopy (FTIR), field emission gun-scanning electron microscopy (FEG-SEM), X-ray photoelectron spectroscopy (XPS), and X-ray diffraction were employed in order to evaluate the morphology, structure, and crystalline phase of the TiO_2 layer obtained. Raman spectroscopy was employed to evaluate the integrity of the CNTs before and after the coating process. Finally, thermogravimetric analysis was employed to assess the TiO_2-coated MWCNT stability in the O_2 atmosphere.

2. Materials and Methods

2.1. Carbon Nanotube Functionalization. Baytubes® C 150 P multiwalled carbon nanotubes (MWCNTs), produced by Bayer MaterialScience-Germany by the CVD process, with purity greater than or equal to 95%, were used. The MWCNTs have internal and external diameters of the order of 4 and 13 nm, respectively, with a length greater than 1 μm. The MWCNTs were acid treated in 60 mL of 1 : 3 ($v : v$) of analytical grade nitric acid 65% PA and sulfuric acid PA-ACS for 6 hours under magnetic stirring. The resulting mixture was washed with deionized water until a neutral pH was reached and dried at 80°C for 15 hours.

2.2. Synthesis of the TiO_2-Coated MWCNTs. The route to produce TiO_2 shell supported over the MWCNT core was carried out according to the modified surfactant wrapping sol-gel method reported by Gao et al. [26] and is shown in a flowchart in Figure 1. This procedure, when repeated (Cycles I, II, and III), is able to produce thicker TiO_2 coatings.

In the first cycle (Cycle I), MWCNTs were mixed with 2% wt. of sodium dodecyl sulphate (Synth) in aqueous solution and kept in an ultrasonic bath for 3 hours. The final concentrations of MWCNTs in Milli-Q water were 4, 6, and 8 mg/mL. Then, 20 mL of absolute ethyl alcohol 99.8% P.A. was added to the aqueous solution and stirred for additional 0.5 hours, in order to form a MWCNT solution. In parallel, titanium isopropoxide (Aldrich) was mixed to 15 mL of absolute ethyl alcohol 99.8% P.A. and glacial acetic acid 99.8% P.A. under stirring for 0.5 hours, to form a TiO_2 precursor solution. Then the TiO_2 precursor solution was added dropwise in the CNT solution under vigorous stirring that was kept for 2 hours in order to complete the coating reaction. The final percentage of MWCNTs, related to the total weight of the MWCNT-coated TiO_2 hybrid nanocomposite, was estimated to be 16, 23, and 28 by weight (wt.%), when the concentrations of MWCNTs in Milli-Q water were 4, 6, and 8 mg/mL, respectively. Ammonium hydroxide P.A. (Synth) was added dropwise until pH 9 was reached. Finally, 10 mL of absolute ethyl alcohol was added, and the mixture was kept under stirring for another 0.5 hours. Subsequently, the solution was vacuum filtered using a cellulose acetate membrane and washed with 200 mL of absolute ethyl alcohol. The drying process was carried out for 15 hours in an oven at 60°C to obtain the powdered core-shell structure of TiO_2-coated MWCNTs, named CI (Cycle I).

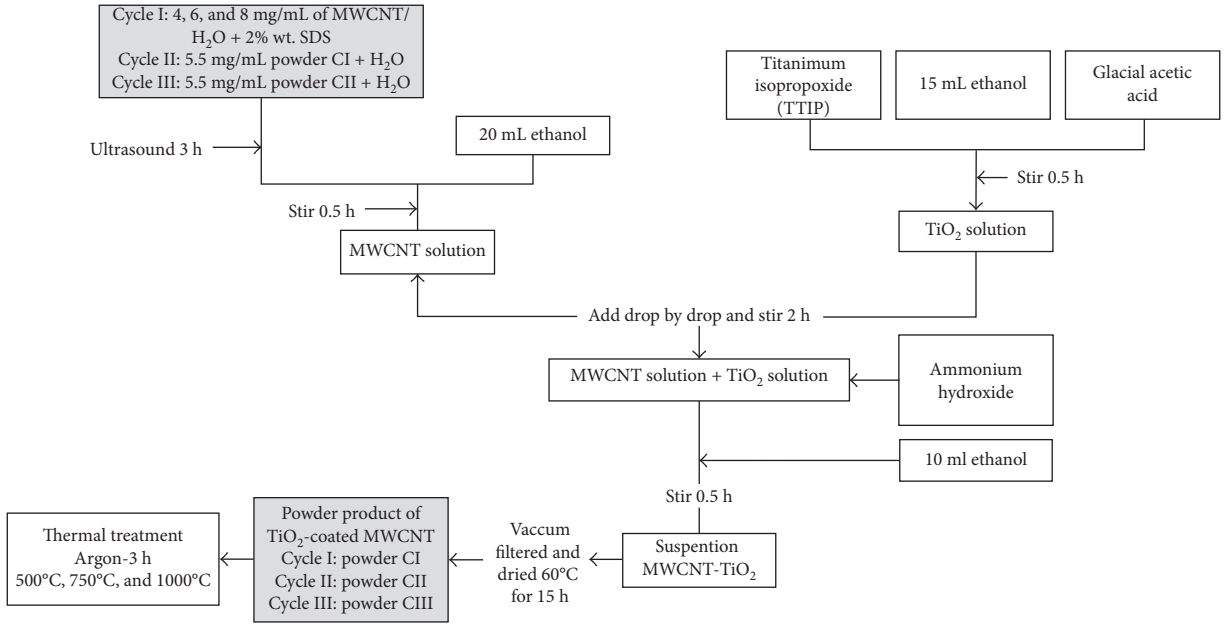

Figure 1: Flowchart describing the carbon nanotube-coating process with TiO_2.

For the second cycle (Cycle II), powder CI (obtained in Cycle I with 28 wt.% of MWCNTs) was mixed with Milli-Q water (5.5 mg/mL) and dispersed in an ultrasonic bath for 3 hours. The obtained suspension was subjected to the same process described above for the CI powder. For the product of the Cycle II (named CII), the final percent of MWCNTs, related to the total weight of the MWCNT-coated TiO_2 nanocomposite, was estimated from the mass balance of the precursors to be 8.23 wt.%. For the third cycle (Cycle III), the overall process is repeated, starting from the powder CII and the final percent of MWCNTs, related to the total weight of the MWCNT-coated TiO_2 nanocomposite, was estimated to be 2.32 wt.%.

As the obtained TiO_2 coating is amorphous and unstable, powders obtained from Cycles I, II, and III were heat treated at 500°C, 750°C, and 1000°C for 3 hours in an argon atmosphere, in order to crystallize the coating layer and to reduce its pore size and surface area.

2.3. Samples Analysis. The starting (pristine) MWCNTs, the functionalized MWCNTs, and the hybrid MWCNT/TiO_2 nanocomposites after calcination were characterized by X-ray diffraction, the later to evaluate the crystallinity degree of the coating. X-ray analysis was performed in a Rigaku X-ray diffractometer, model Ultima IV, using Cu Kα radiation ($\lambda = 1.54178$ Å), voltage of 40 kV, and current of 30 mA. Multiple detectors (fast detection mode) were used at steps of 0.01° and speed of 5°/min, resulting in a high signal level. The nature of the surface molecular groups of MWCNTs before and after functionalization and calcined TiO_2 coating was characterized by a Shimadzu IR-affinity-1 FTIR spectrophotometer, in the region of 4000 to 500 cm^{-1} with a resolution of 4 cm^{-1} after 32 accumulations. The data were acquired in transmittance mode, using the KBr pellet technique. Complementary information about the molecular structure of the functionalized and TiO_2-coated MWCNTs, after calcination, was obtained by X-ray photoelectron spectroscopy (XPS), using a Kratos Axis Ultra XPS, operating in an ultra-high vacuum (approximately 10^{-7} Pa). A monochromatic Al X-ray source was used, with energy of 1486.5 eV and power of 150 W, given by the voltage of 15 kV. The emitted photoelectrons were collected in a hemispherical analyzer with 15 µm of spatial resolution. The energy resolution of the equipment is 0.58 eV. Analysis from the samples was performed in the survey mode, followed by scans located in the regions of C 1s, O 1s, and Ti 2p, corresponding to the locations of the carbon, oxygen, and titanium peaks, respectively. Raman spectroscopy was performed in samples using a Horiba LabRAM microscope with 514 nm lasers, in order to identify typical scatters from carbon structures, as well as from the coating structure after calcination. Spectra were collected from 3 accumulations of 30 seconds each, in the range of 50 to 2000 cm^{-1}.

The microstructure of the MWCNT/TiO_2 core/shell nanocomposites was analyzed using a Tescan model Mira 3 field emission gun-scanning electron microscope (FEG-SEM).

The thermal stability of the samples was evaluated from thermal gravimetric analyzes, using a NETZSCH STA 449 F1 Jupiter thermal analysis equipment (TG-DSC/DTA) with a heating rate of 10°C/min in the range of 200 to 1000°C, in synthetic air (20% O_2 and 80% N_2) atmosphere with a flow of 20 mL/min.

3. Results and Discussion

3.1. Scanning Electron Microscopy. The FEG-SEM images of nanotubes after sol-gel TiO_2-coating processing are presented in Figure 2. It can be observed that high-quality deposits have been obtained. For coating Cycle I, the

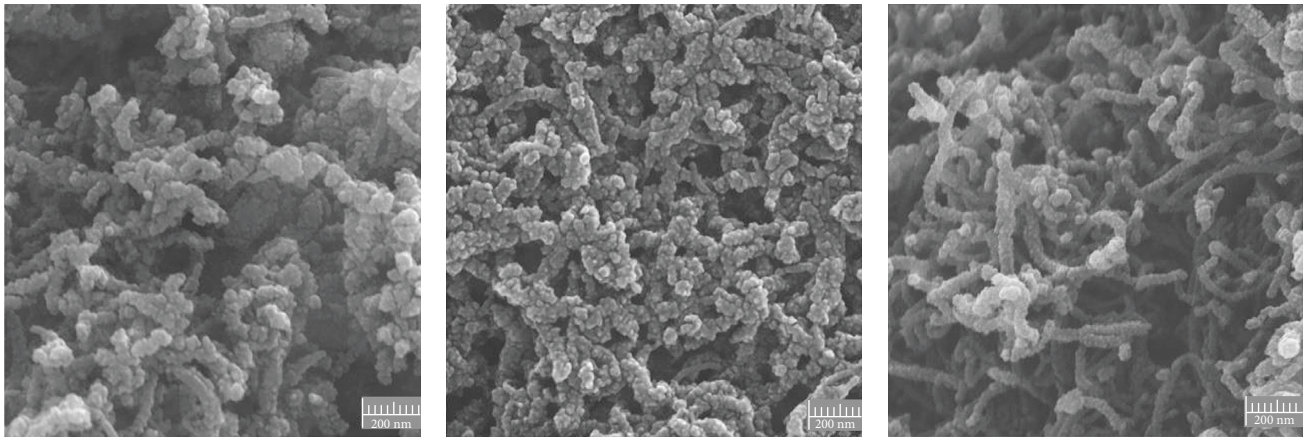

(a) (b) (c)

Figure 2: FEG-SEM images of core/shell structures of TiO_2-coated MWCNT nanocomposites, obtained from different MWCNT concentrations in water during the sol-gel process: (a) 4 mg/mL, (b) 6 mg/mL, and (c) 8 mg/mL.

effect of varying the final concentration of MWCNTs in aqueous solution (4, 6, and 8 mg/mL) is also observed. From Figure 2(a), it is observed that the lower the MWCNT concentration (4 mg/mL), the thicker is the TiO_2 coating. Besides the coating formation, a large amount of isolated TiO_2 nanoparticles are formed at this lower MWCNT concentration, as less superficial area of substrate (core) is available for the coating formation. Figure 2(b) shows that when the MWCNT concentration in the aqueous solution increases to 6 mg/mL, the MWCNTs are completely coated, similarly to the previous sample, but with a smaller amount of isolated TiO_2 nanoparticles. Finally, when the concentration of MWCNTs in water increases to 8 mg/mL, the nanotubes are observed to be completely coated with a thin layer of TiO_2 and no isolated particles are present. In such a condition, it seems that the mass relation between MWCNT core and TiO_2 shell is optimized.

Once a mass relation of MWCNTs to TiO_2 that results in a homogeneous coating and less isolated particles was established, attempts to obtain thicker deposits of TiO_2 over the nanotubes surface have been made by increasing the number of coating cycles. Figure 3 shows the aspect of MWCNTs submitted to two coating cycles and calcined at 500 and 1000°C. It can be easily observed that the second cycle produces much thicker layers not uniformly covering the nanotubes. The same is observed in Figure 3(b). However, when comparing the coatings after calcination at 500 and 1000°C (Figures 3(a) and 3(b), resp.), the changes in the layer morphology treated at higher temperature are easily seen. The layer becomes denser and particles size increase from few nanometers to the order of hundred nanometers, forming a necklace arrangement. These changes are related to the anatase to rutile phase transformation and are accompanied by a significant reduction in the specific surface area [28].

3.2. FTIR Analysis. After the acid functionalization, functional groups containing oxygen such as hydroxyl (-OH), carboxyl (-COOH), and carbonyl (C=O) are expected to form over the nanotubes surface. In order to verify the successful formation of such groups, FTIR spectroscopy was employed. The results are presented in Figure 4 and summarized in Table 1.

From Figure 4 and Table 1, it can be observed that acid functionalization was successful, as several functional groups were formed on the MWCNT surface. The acid treatment breaks few C=C bonds, forming other C, H, and O groups tightly attached to the nanotubes [32]. Furthermore, structural defects eventually present are sites for functional groups to form. The functional groups formed are a basis for the TiO_2 layer anchoring in the subsequent coating treatment, as observed by the presence of the band at 500 cm^{-1} in the coated sample, associated with the titanium Ti-O-Ti stretch bonding from the titanium oxide formed after calcination [34].

3.3. X-Ray Photoelectron Spectroscopy. Although the TiO_2 formation was identified by FTIR analysis, its tight bonding to the MWCNT surface has to be verified by other techniques. XPS measurements were made to study the chemical state of the MWCNT/TiO_2 core/shell nanocomposite. The formation of TiO_2 attached to the surface of the functionalized nanotubes is clearly shown by the data from Ti2p binding energy (Figure 5(a)). After deconvolution, the measured energies for Ti^{+4} bonding were 459.56 eV for Ti2p 3/2 and 465.28 eV for Ti2p 1/2. The difference between these two peaks was 5.72 eV. Theoretically, the TiO_2 bonding energies (Ti2p 3/2 and Ti2p 1/2) are centered at 458.7 and 464.4 eV, and their difference is 5.7 eV. The small positive displacement observed in this work suggests that an electronic interaction between TiO_2 and the MWCNT substrate was established [37], resulting from a close interaction between the nanotubes and the oxide coating.

Figure 5 also shows the analysis for (Figure 5(b)) O 1s and (Figure 5(c)) C 1s energy binding of the TiO_2-coated

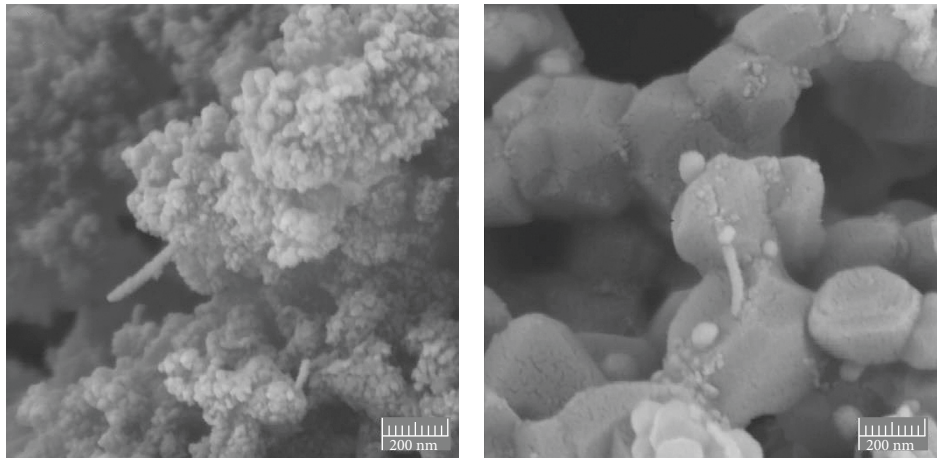

(a) (b)

Figure 3: FEG-SEM images of core/shell structures of TiO_2-coated MWCNT composites with two coating cycles thermal treated at (a) 500°C and (b) 1000°C.

MWCNT sample. The O 1s spectrum can be adjusted to three peaks, where the main peak at 530.9 eV corresponds to the Ti-O network oxygen. The other two peaks with binding energies of 531.7 and 532.9 eV are assigned to the O-H and C=O groups, respectively. Similarly to the Ti 2p spectrum, the main peak in O 1s is slightly displaced (0.9 eV), as a result of the interaction and consequent surface charge transfer between TiO_2 and MWCNTs [37]. The C 1s spectrum was adjusted to four peaks, representing the C=C binding energy of MWCNTs of 284.7 eV, as well as C-O, C=O, and COO- energies of 286.1, 287.9, and 290.1 eV, respectively. These results reinforce the results from FTIR analysis, evidencing the formation of functional groups on the MWCNT surface after acid functionalization. It is very important to note that, even after calcination at 1000°C, there is no evidence of carbon replacing oxygen atoms in the lattice of TiO_2, as the formation of O-Ti-C bonds commonly represented in the C 1s spectrum by a peak at 282.5 eV [34]. Additionally, Figure 5(d) shows the composite valence band (VB), where no additional electronic states are shown above the TiO_2 edge valence band, discarding any possible carbon doping in the TiO_2 network [38, 39].

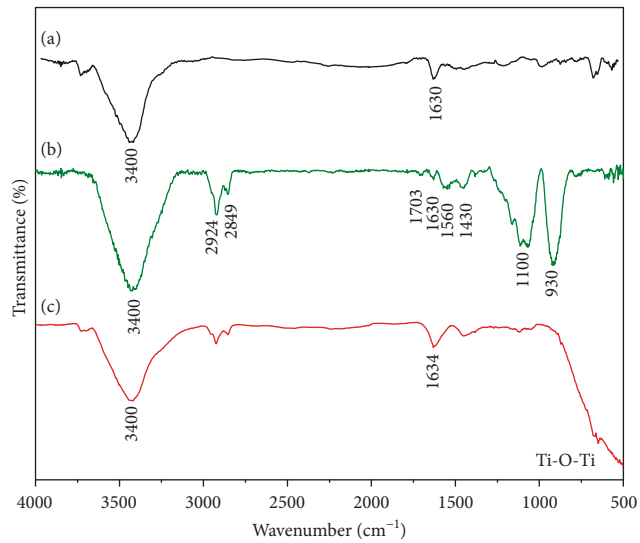

Figure 4: FTIR spectra of (a) pristine, (b) oxidized (functionalized), and (c) TiO_2-coated MWCNTs with I coating cycle after calcination at 1000°C.

3.4. X-Ray Diffraction. After calcination at different temperatures, the presence of a crystalline TiO_2 layer was confirmed by X-ray diffraction, and the results are shown in Figure 6. Comparison of the diffraction patterns of MWCNT/TiO_2 core/shell nanocomposite samples treated at 500, 750, and 1000°C shows that the crystal form of the coating layer changes from totally anatase to totally rutile, as the calcination temperature increases. At the intermediate temperature of 750°C, a mixture of both crystalline structures is observed.

It is also important to note that no characteristic peaks of MWCNTs were found. The proximity of the most intense anatase (101) peak at $2\theta = 25.2^\circ$ with the most intense (002) graphitic MWCNT peak at $2\theta = 25.9^\circ$ impairs the nanotube identification by X-ray diffraction in the coated samples. However, the presence of MWCNTs in the nanocomposites was further confirmed by Raman analysis as discussed later.

A rough approximation of the crystallite size of the samples was calculated by the well-known Scherrer equation: $D = k\lambda/(\beta\cos\theta)$, where D is the crystallite particle size, k is a constant of 0.9, λ is the wavelength (nm) of the X-rays used, β is the peak full width at half maximum (FWHM), and θ is the Bragg angle [34]. Calculations show that the crystallite size for the samples of II cycles calcined at 500°C was about 5 nm, increasing to about 87 nm in samples calcined at 750°C, and more significantly to about 118 nm after calcination at 1000°C. These results indicate that the phase transformation from anatase to rutile induced both grain growth and probably surface area reduction and are in agreement with the literature [28] and with scanning electron microscopy results.

Table 1: FTIR bands observed for pristine, acid-functionalized, and TiO_2-coated MWCNTs.

Band (cm^{-1})	Interpretation	Pristine	Acid functionalized	TiO_2 coated
3400	OH stretching vibrations of isolated surface –OH moieties and in sorbed water [31]	x	x	x
2924	Asymmetric stretching of CH bonds located on the MWCNT surface defects [32]	—	x	—
2849	Symmetric stretching of CH bonds located on the MWCNT surface defects [32]	—	x	—
1730	C=O bonds related to the carboxyl group COOH [33]	—	x	—
1630	OH stretch of adsorbed water and Ti-OH [34]	x	x	x
1560	C-O carboxylate anion stretch mode [33]	—	x	—
1430	O-H deformation vibrations [31]	—	x	—
1100	C-O stretch [31, 35]	—	x	—
930	O-H stretch [36]	—	x	—
500	Ti-O-Ti stretch [34]	—	—	x

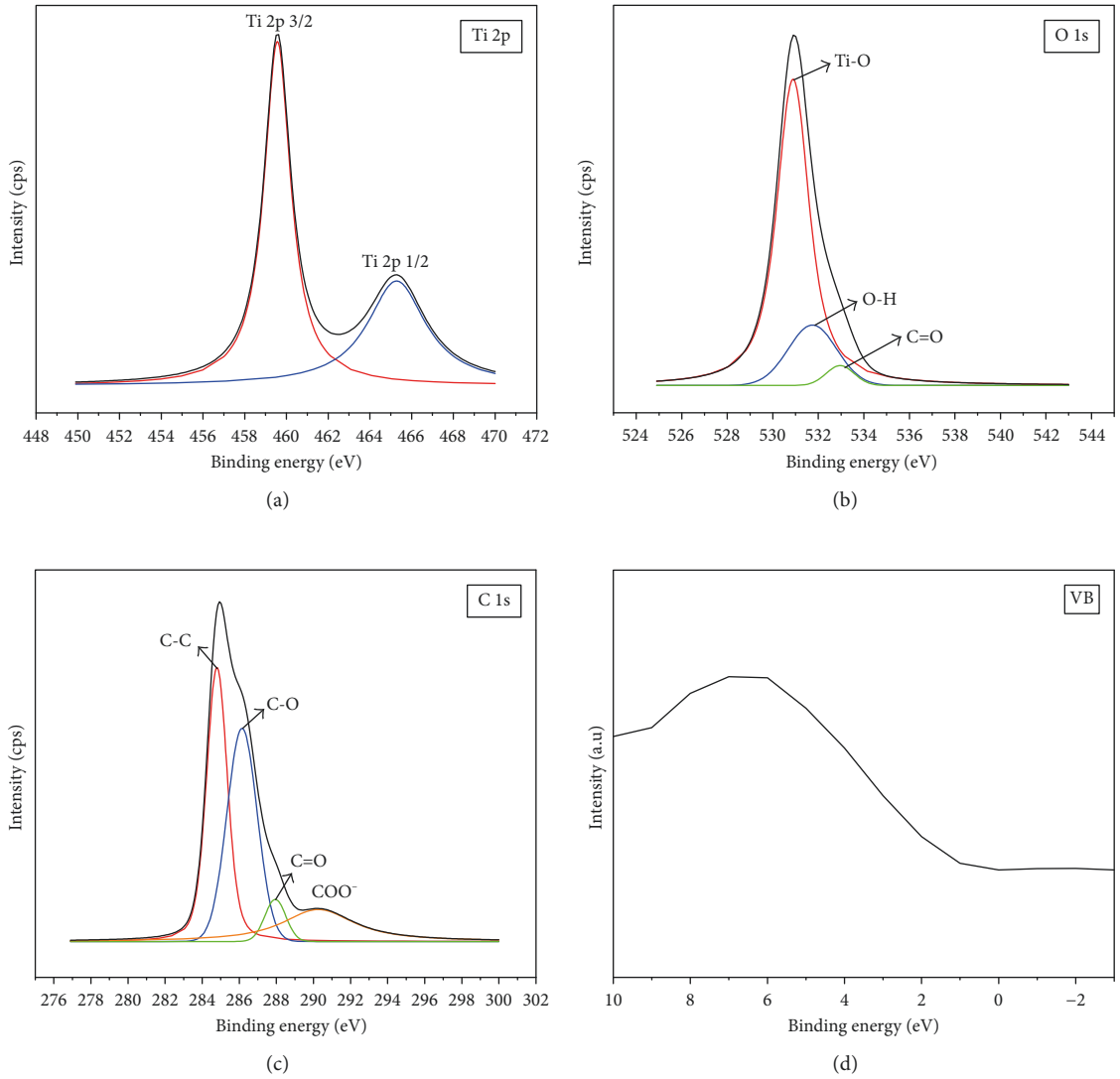

Figure 5: High-resolution XPS spectra of (a) Ti 2p, (b) O 1s, (c) C 1s, and (d) XPS valence band for TiO_2-coated MWCNTs with II coating cycles after calcination at 1000°C.

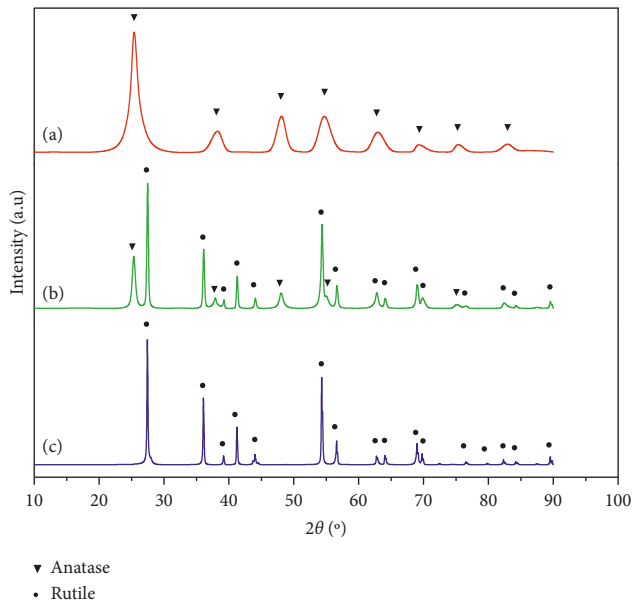

FIGURE 6: X-ray diffraction spectra for TiO_2-coated MWCNTs with II coating cycles and calcined at (a) 500°C, (b) 750°C, and (c) 1000°C.

3.5. Raman Spectroscopy. Figure 7(a) presents the Raman spectra obtained for the pristine MWCNTs. The *D* and *G* bands were identified at their typical positions: 1337.37 cm^{-1} and 1576.31 cm^{-1}, respectively. After acid functionalization, no shifting was observed on these *D* and *G* peak bands. However, their intensity and width changes slightly. Perfect highly ordered graphitic structures do not produce scatter *D*-band, which is associated with structural defects. Consequently, the *D*/*G* ratio is commonly used to assess the crystalline quality of carbon-based materials. In the present work, *D*/*G* ratio increases from 1.24 (pristine MWCNTs) to 1.36 after acid functionalization, indicating that the external wall of the nanotubes is damaged in a certain extension in order to introduce the functional groups. However, it is to be pointed out that this increase was not so intense.

Figure 7(b) shows the spectra for the MWCNT/TiO_2 nanocomposites calcined at different temperatures. Typical E_g (142 cm^{-1}), B_{1g} (399 cm^{-1}), A_{1g} (518 cm^{-1}), and E_g (641 cm^{-1}) scattering bands of anatase are present in samples treated at 500°C. At 750°C, scattering bands of B_{1g} (145 cm^{-1}), E_g (446 cm^{-1}), A_{1g} (612 cm^{-1}), and the multiphoton process (230 cm^{-1}) of rutile [40] start to be visible and are predominate after calcination at 1000°C. These results fully agree with the results from X-ray diffraction. Still referring to Figure 7(b), it is possible to observe the presence of the D and G bands from the functionalized MWCNT substrate, located between 1342–1359 cm^{-1} and 1583–1594 cm^{-1}, respectively. Both bands are slightly shifted to larger wavenumbers, when comparing to Figure 7(a). According to the literature [41, 42], upshift of the *D* band can be related to stresses induced by the presence of TiO_2 shell on the surface of the MWCNT core, and the upshift of the *G* band is due to a high-structural interaction (bonding) between the TiO_2 and the MWCNTs [43, 44].

Gui et al. [42] found in a MWCNT/TiO_2 composite that the intensity ratio of main anatase Eg mode related to the intensity of graphene band (I_A/I_G) reduces, as the ratio of TiO_2 : MWCNTs increases. In the present work, in samples with pure anatase (calcined at 500°C), the I_A/I_G ratio obtained was observed to increase as the number of coating cycles increases. In samples subjected to a single coating cycle (TiO_2 : MWCNT ratio of 1 : 0.4), I_A/I_G ratio obtained was 0.80. I_A/I_G ratio obtained after two and three cycles (TiO_2 : MWCNT ratio of 1 : 0.115 and 1 : 0.0325) was found to be 6.32 and 9.35, respectively. These results are consistent with the results of Gui and et al. and reveal that the high intensity of the anatase E_g scattering band is related to the excess of TiO_2 related to MWCNTs [42].

As far as the I_D/I_G ratio is concerned, after calcination at 500°C, it was found to decrease to the range of 0.74–0.81, when comparing to pristine and acid-functionalized MWCNTs (1.24 and 1.36, resp.). This behavior can be attributed to the thermal-induced rearrangement of the carbon structure [45]. Based on this result, it would be expected that calcination at higher temperatures would continuously decrease the I_D/I_G ratio. However, an opposite effect was observed. After calcination at 750°C, I_D/I_G obtained was in the range of 0.83–0.95, and 0.98–1.11 after calcination at 1000°C. This behavior can be related to the anatase to rutile phase transformation, evidenced from X-ray diffraction and Raman spectroscopy. This transformation is reconstructive; that is, it requires rearrangement of the Ti-O atoms to fit to the new structure. Furthermore, significant grain growth and densification (reducing the specific surface area) are expected [28]. As Ti-O atoms are tightly bonded to the MWCNT surface, stresses associated with the TiO_2 reconstruction should be transferred to the nanotubes, increasing the MWCNT network distortion and consequently the intensity of the *D* scatter band.

3.6. Thermogravimetry. TGA analysis was performed in order to estimate the final amount of MWCNTs in the

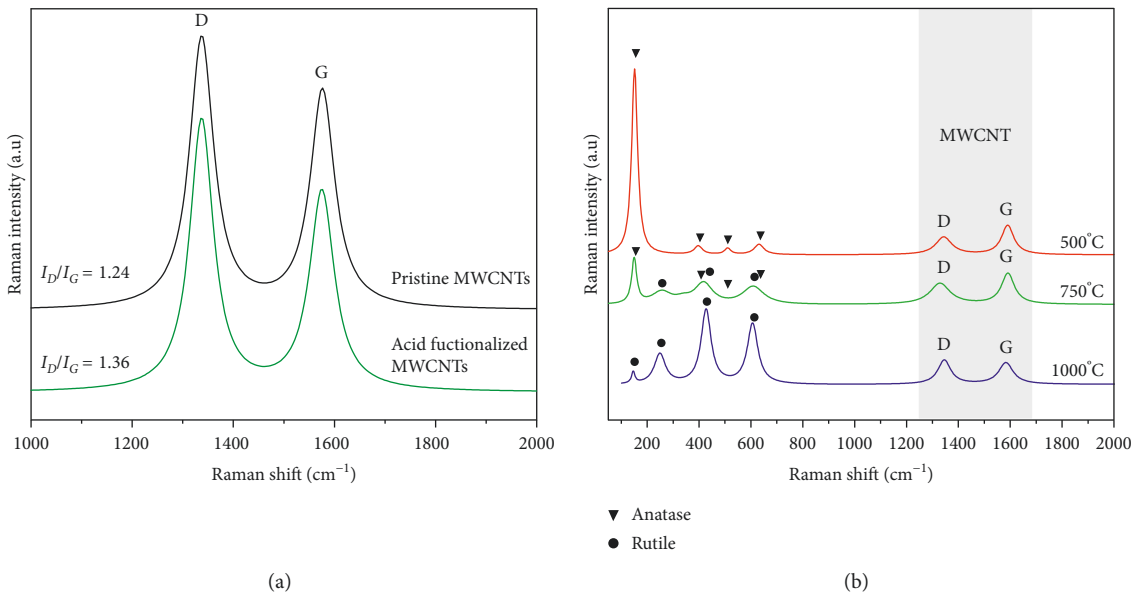

(a) (b)

Figure 7: Raman spectra for pristine and acid functionalized MWCNTs. (b) TiO_2-coated MWCNTs with II coating cycles calcined at 500°C, 750°C, and 1000°C.

nanocomposite, and consequently the level of thermal protection offered by the layer of TiO_2 in different thicknesses and structure types. Eventual MWCNT oxidation is expected to form CO_2 gas, leaving the sample and resulting in composite weight loss as a function of temperature (Figure 8).

From the TGA results, several observations are worth to mention. All samples presented a mass loss up to about 400°C, which can be attributed to the decomposition of surfactant residues still present in the sample. This is more evident in the samples calcined at smaller temperatures: 500°C and 750°C. The thermal decomposition of SDS is very slow [46] and presents a mass loss also at about 750°C, due to the final decomposition of $NaSO_4$, which is very stable up to temperatures around 800°C [47]. After about 450°C, the samples start to present a significant mass loss, being more severe as the calcination temperature decreases. This mass loss is attributed to the decomposition of MWCNTs into CO_2 by the O_2 atmosphere. The oxidation peak, observed in DTG curves, occurs at about 550°C. The constant levels observed after 600°C in TGA curves should correspond to the complete oxidation of nanotubes. An estimative of the remaining carbon content in the samples can be made comparing this weight loss during TGA with the total weight of the MWCNT-coated TiO_2 nanocomposite (based on the mass balance of the precursors), assuming that loses are related to the MWCNTs. This hypothesis is feasible, as the TiO_2 coating is very stable, even after calcination at only 500°C, and the anatase to rutile phase transformation is not associated with changes in mass. This analysis, presented in Table 2, enables to quantitatively evaluate the protection level of the TiO_2 coating as a function of the layer thickness and calcination temperature. For the sample submitted to two coating cycles, calcined at 500 and 750°C, these ratios were 1.00 and 1.15, respectively, which are lower than the values of the sample submitted to only one coating cycle and calcined at the same temperatures: 1.12 and 1.30, respectively. These results can be explained by the lack of homogeneity of the coatings obtained in Cycle II, as shown in Figure 3. However, it is possible to note that the protection level expressed by the ratio between initial weight and weight loss drastically increases from around 1.00 to 7.48, when comparing the sample coated by two coating cycles of TiO_2 calcined at 500°C with the sample coated by three coating cycles calcined at 1000°C. Similar results were found by Li. et al. [27] in TiO_2/MWCNT nanocomposites obtained by the sol-gel process using different titanium precursors and calcination at 500°C. However, the authors suggest that the remaining carbon after TGA analysis is related to elemental diffusion from the substrate into the TiO_2-coating structure during calcinations at 500°C, through a transfer-doping mechanism.

As shown in the FEG-SEM images and from XRD calculated crystallite size, the increase in the calcination temperature changes the morphology of the TiO_2-coating layer, making it denser and with lesser superficial area, favoring its growth. In fact, the TGA results showed that the higher the calcination temperature, the lower the MWCNT loss. Manivannan et al. [48] found that sintering MWCNTs coated with zirconia improved their resistance to oxidation, and this improvement is related to the proper selection of the sintering temperature. On the other hand, Inam et al. [30] found that the thicker the alumina layer deposited over MWCNTs, the better protection against oxidation it provides. However, it decreases the mechanical properties of the resulting composite by making the coated nanotubes more brittle. It is worth to reinforce that, contrarily to the work of Li et al. [27], in the present work the XPS analysis showed no evidences of carbon doping in the TiO_2 structure, strongly suggesting that the remaining carbon refers to intact, not

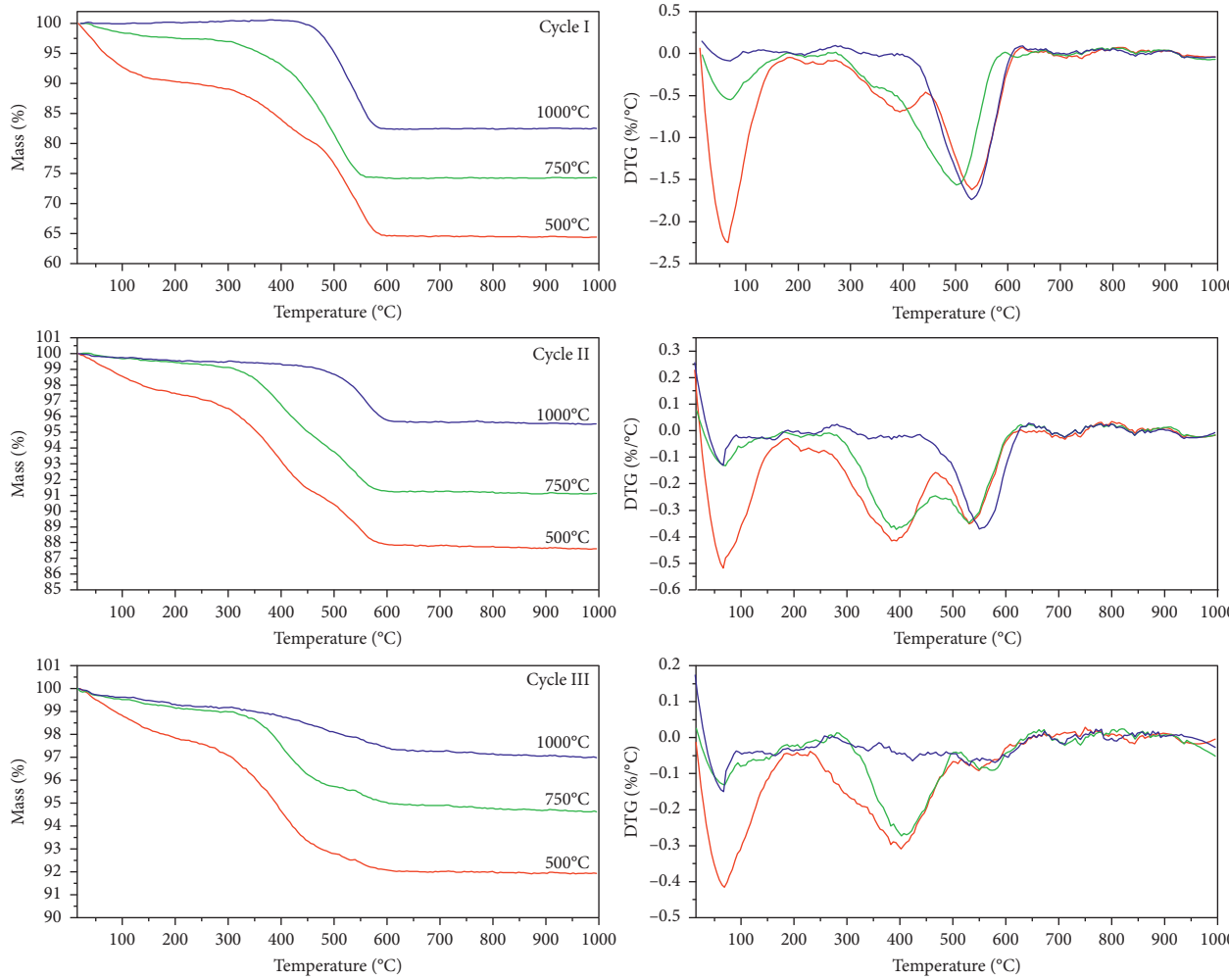

Figure 8: TGA and DTG curves of TiO_2-coated MWCNT composites prepared with I, II, and III coating cycles and calcined at 500°C, 750°C, and 1000°C.

Table 2: Carbon content in TiO_2-coated MWCNT composites.

Sample	Initial MWCNT %wt.[1]	Calcination temp. (°C)	TGA %wt. loss[2] (%wt[1]/%wt[2])
Cycle I	28.57	500	25.47 (1.12)
		750	21.88 (1.30)
		1000	17.22 (1.65)
Cycle II	8.23	500	8.21 (1.00)
		750	7.11 (1.15)
		1000	3.58 (2.29)
Cycle III	2.32	500	0.61 (3.80)
		750	0.40 (5.80)
		1000	0.31 (7.48)

Notes. The carbon contents presented here correspond to [1]the values before sample fabrication (percent of MWCNTs, related to the total weight of the MWCNT-coated TiO_2 nanocomposite) and [2]those determined by TGA analysis, respectively.

damaged MWCNTs, protected from oxidation by a dense and continuous layer of TiO_2 that completely coats the nanotube surface and acting as an efficient thermal shielding. Furthermore, as observed from the results depicted in Table 2, the MWCNT protection improves as the coating thickness increases. This result is similar to the results of Inam et al. [30], as already mentioned, and is probably related to the fact that gaseous oxygen would take longer times to reach the MWCNT surface. Consequently, it seems to be feasible to coat MWCNTs with TiO_2 layers in order to protect them from oxidation during the high temperatures involved in MMC processing. Besides, it is expected that the TiO_2 coating layer formed over the MWCNT surface can improve their dispersion and

adherence into the metallic matrix. With their integrity preserved, carbon nanotubes can fully contribute to strength in MMCs.

4. Conclusions

In this work, MWCNTs were uniformly coated with a TiO_2 continuous layer with core/shell structure, through the sol-gel method. The layer thickness formed could be controlled by the repetition of the coating cycles, and a stable and dense coating layer could be reached after calcination at 1000°C. Results from of X-ray diffraction and Raman spectroscopy confirm that the layer structure continuously changes from completely anatase to completely rutile, as the calcination temperature increases from 500 to 1000°C. TiO_2 coating formation was also confirmed by XPS, without any C doping in the TiO_2 network. The thermal protection effect of the TiO_2 layer against MWCNT oxidation was confirmed by TGA curves, showing that this protection is more efficient as the layer thickness increases, as well as the calcination temperature. The thermal protection of the MWCNTs is attributed to the fact that high-temperature calcination contributes to pore closure and densification of the TiO_2 layer, reducing the contact between oxygen and the substrate.

The results shown in this work can open new opportunities to fabricate metallic matrix composite materials reinforced by MWCNTs without damaging their structure during the high temperatures to which they are exposed during MMC processing.

Conflicts of Interest

The authors declare that they have no conflicts of interest regarding the publication of this paper.

Acknowledgments

The authors are thankful to the Associated Laboratory for Sensors and Materials (LAS-INPE–Brazil), for the FEG-SEM images, Raman spectroscopy, and XPS analysis and to CNPq for the financial support (Process no. 443395/2014-4).

References

[1] S. Iijima, "Helical microtubules of graphitic carbon," *Nature*, vol. 354, no. 6348, pp. 56–58, 1991.

[2] S. C. Tjong, "Recent progress in the development and properties of novel metal matrix nanocomposites reinforced with carbon nanotubes and graphene nanosheets," *Materials Science and Engineering: R: Reports*, vol. 74, no. 10, pp. 281–350, 2013.

[3] B. Boesl, D. Lahiri, S. Behdad, and A. Agarwal, "Direct observation of carbon nanotube induced strengthening in aluminum composite via in situ tensile tests," *Carbon*, vol. 69, pp. 79–85, 2014.

[4] H. Kwon, M. Estili, K. Takagi, T. Miyazaki, and A. Kawasaki, "Combination of hot extrusion and spark plasma sintering for producing carbon nanotube reinforced aluminum matrix composites," *Carbon*, vol. 47, no. 3, pp. 570–577, 2009.

[5] L. Ci, Z. Ryu, N. Y. Jin-Phillipp, and M. Rühle, "Investigation of the interfacial reaction between multi-walled carbon nanotubes and aluminum," *Acta Materialia*, vol. 54, no. 20, pp. 5367–5375, 2006.

[6] A. M. K. Esawi, K. Morsi, A. Sayed, A. A. Gawad, and P. Borah, "Fabrication and properties of dispersed carbon nanotube-aluminum composites," *Materials Science and Engineering: A*, vol. 508, no. 1-2, pp. 167–173, 2009.

[7] H. J. Choi, G. B. Kwon, G. Y. Lee, and D. H. Bae, "Reinforcement with carbon nanotubes in aluminum matrix composites," *Scripta Materialia*, vol. 59, no. 3, pp. 360–363, 2008.

[8] C. Deng, X. Zhang, D. Wang, Q. Lin, and A. Li, "Preparation and characterization of carbon nanotubes/aluminum matrix composites," *Materials Letters*, vol. 61, no. 8-9, pp. 1725–1728, 2007.

[9] C. F. Deng, D. Z. Wang, X. X. Zhang, and A. B. Li, "Processing and properties of carbon nanotubes reinforced aluminum composites," *Materials Science and Engineering: A*, vol. 444, no. 1-2, pp. 138–145, 2007.

[10] L. Wang, H. Choi, J. M. Myoung, and W. Lee, "Mechanical alloying of multi-walled carbon nanotubes and aluminium powders for the preparation of carbon/metal composites," *Carbon*, vol. 47, no. 15, pp. 3427–3433, 2009.

[11] R. Pérez-Bustamante, I. Estrada-Guel, P. Amézaga-Madrid, M. Miki-Yoshida, J. M. Herrera-Ramírez, and R. Martínez-Sánchez, "Microstructural characterization of Al-MWCNT composites produced by mechanical milling and hot extrusion," *Journal of Alloys and Compounds*, vol. 495, no. 2, pp. 399–402, 2010.

[12] A. M. K. Esawi, K. Morsi, A. Sayed, M. Taher, and S. Lanka, "Effect of carbon nanotube (CNT) content on the mechanical properties of CNT-reinforced aluminium composites," *Composites Science and Technology*, vol. 70, no. 16, pp. 2237–2241, 2010.

[13] A. Esawi and K. Morsi, "Dispersion of carbon nanotubes (CNTs) in aluminum powder," *Composites Part A: Applied Science and Manufacturing*, vol. 38, no. 2, pp. 646–650, 2007.

[14] A. M. K. Esawi and M. A. El Borady, "Carbon nanotube-reinforced aluminium strips," *Composites Science and Technology*, vol. 68, no. 2, pp. 486–492, 2008.

[15] D. N. Travessa and M. Lieblich, "Dispersion of carbon nanotubes in AA6061 aluminium alloy powder by the high energy ball milling process," *Materials Science Forum*, vol. 802, pp. 90–95, 2014.

[16] M. Rashad, F. Pan, J. Zhang, and M. Asif, "Use of high energy ball milling to study the role of graphene nanoplatelets and carbon nanotubes reinforced magnesium alloy," *Journal of Alloys and Compounds*, vol. 646, pp. 223–232, 2015.

[17] D. K. Lim, T. Shibayanagi, and A. P. Gerlich, "Synthesis of multi-walled CNT reinforced aluminium alloy composite via friction stir processing," *Materials Science and Engineering: A*, vol. 507, no. 1-2, pp. 194–199, 2009.

[18] H. Kurita, H. Kwon, M. Estili, and A. Kawasaki, "Multi-walled carbon nanotube-aluminum matrix composites prepared by combination of hetero-agglomeration method, spark plasma sintering and hot extrusion," *Materials Transactions*, vol. 52, no. 10, pp. 1960–1965, 2011.

[19] S. R. Bakshi, A. K. Keshri, and A. Agarwal, "A comparison of mechanical and wear properties of plasma sprayed carbon nanotube reinforced aluminum composites at nano and macro scale," *Materials Science and Engineering: A*, vol. 528, no. 9, pp. 3375–3384, 2011.

[20] T. Laha and A. Agarwal, "Effect of sintering on thermally sprayed carbon nanotube reinforced aluminum nanocomposite,"

Materials Science and Engineering: A, vol. 480, no. 1-2, pp. 323–332, 2008.

[21] T. Laha, Y. Chen, D. Lahiri, and A. Agarwal, "Tensile properties of carbon nanotube reinforced aluminum nanocomposite fabricated by plasma spray forming," *Composites Part A: Applied Science and Manufacturing*, vol. 40, no. 5, pp. 589–594, 2009.

[22] Y. Chen, F. Lu, K. Zhang et al., "Laser powder deposition of carbon nanotube reinforced nickel-based superalloy Inconel 718," *Carbon*, vol. 107, pp. 361–370, 2016.

[23] S. R. Bakshi, V. Singh, S. Seal, and A. Agarwal, "Aluminum composite reinforced with multiwalled carbon nanotubes from plasma spraying of spray dried powders," *Surface and Coatings Technology*, vol. 203, no. 10-11, pp. 1544–1554, 2009.

[24] J. K. Park and J. P. Lucas, "Moisture effect on SiCp/6061 Al MMC: dissolution of interfacial Al_4C_3," *Scripta Materialia*, vol. 37, no. 4, pp. 511–516, 1997.

[25] I. Jo, S. Cho, H. Kim, B. M. Jung, S.-K. Lee, and S.-B. Lee, "Titanium dioxide coated carbon nanofibers as a promising reinforcement in aluminum matrix composites fabricated by liquid pressing process," *Scripta Materialia*, vol. 112, pp. 87–91, 2016.

[26] B. Gao, C. Peng, G. Chen, and G. Lipuma, "Photo-electrocatalysis enhancement on carbon nanotubes/titanium dioxide (CNTs/TiO_2) composite prepared by a novel surfactant wrapping sol–gel method," *Applied Catalysis B: Environmental*, vol. 85, no. 1-2, pp. 17–23, 2008.

[27] Z. Li, B. Gao, G. Z. Chen, R. Mokaya, S. Sotiropoulos, and G. Li Puma, "Carbon nanotube/titanium dioxide (CNT/TiO_2) core-shell nanocomposites with tailored shell thickness, CNT content and photocatalytic/photoelectrocatalytic properties," *Applied Catalysis B: Environmental*, vol. 110, pp. 50–57, 2011.

[28] D. Eder and A. H. Windle, "Morphology control of CNT-TiO_2 hybrid materials and rutile nanotubes," *Journal of Materials Chemistry*, vol. 18, no. 17, pp. 2036–2043, 2008.

[29] S. Aksel and D. Eder, "Catalytic effect of metal oxides on the oxidation resistance in carbon nanotube–inorganic hybrids," *Journal of Materials Chemistry*, vol. 20, p. 9149, 2010.

[30] F. Inam, T. Vo, and S. Kumara, "Improving oxidation resistance of carbon nanotube nano-composites for aerospace applications," in *Proceedings of 2nd International Conference on Advanced Composite Materials and Technologies for Aerospace Applications*, pp. 1–6, Wrexham, North Wales, UK, June 2012.

[31] L. Stobinski, B. Lesiak, L. Kövér et al., "Multiwall carbon nanotubes purification and oxidation by nitric acid studied by the FTIR and electron spectroscopy methods," *Journal of Alloys and Compounds*, vol. 501, no. 1, pp. 77–84, 2010.

[32] B. Scheibe, E. Borowiak-Palen, and R. J. Kalenczuk, "Oxidation and reduction of multiwalled carbon nanotubes—preparation and characterization," *Materials Characterization*, vol. 61, no. 2, pp. 185–191, 2010.

[33] M. A. Atieh, O. Y. Bakather, B. Al-tawbini, A. A. Bukhari, F. A. Abuilaiwi, and M. B. Fettouhi, "Effect of carboxylic functional group functionalized on carbon nanotubes surface on the removal of lead from water," *Bioinorganic Chemistry and Applications*, vol. 2010, Article ID 603978, 10 pages, 2010.

[34] S. S. Mali, C. a. Betty, P. N. Bhosale, and P. S. Patil, "Synthesis, characterization of hydrothermally grown MWCNT-TiO_2 photoelectrodes and their visible light absorption properties," *ECS Journal of Solid State Science and Technology*, vol. 1, no. 2, pp. M15–M23, 2012.

[35] X. Yan, B. K. Tay, and Y. Yang, "Dispersing and functionalizing multiwalled carbon nanotubes in TiO_2 sol," *Journal of Physical Chemistry B*, vol. 110, no. 51, pp. 25844–25849, 2006.

[36] J. M. Silva-Jara, R. Manríquez-González, F. A. López-Dellamary, J. E. Puig, and S. M. Nuño-Donlucas, "Semi-continuous heterophase polymerization to synthesize nanocomposites of poly(acrylic acid)-functionalized carbon nanotubes," *Journal of Macromolecular Science, Part A*, vol. 52, no. 9, pp. 732–744, 2015.

[37] J. Li, S. Tang, L. Lu, and H. C. Zeng, "Preparation of nanocomposites of metals, metal oxides, and carbon nanotubes via self-assembly," *Journal of the American Chemical Society*, vol. 129, no. 30, pp. 9401–9409, 2007.

[38] S. Wang, L. Zhao, L. Bai, J. Yan, Q. Jiang, and J. Lian, "Enhancing photocatalytic activity of disorder-engineered C/TiO_2 and TiO_2 nanoparticles," *Journal of Materials Chemistry A*, vol. 2, no. 20, p. 7439, 2014.

[39] H. Tan, Z. Zhao, M. Niu et al., "A facile and versatile method for preparation of colored TiO_2 with enhanced solar-driven photocatalytic activity," *Nanoscale*, vol. 6, no. 17, pp. 10216–23, 2014.

[40] J. Yan, G. Wu, N. Guan, L. Li, Z. Li, and X. Cao, "Understanding the effect of surface/bulk defects on the photocatalytic activity of TiO_2: anatase versus rutile," *Physical Chemistry Chemical Physics*, vol. 15, no. 26, pp. 10978–88, 2013.

[41] C.-H. Wu, C.-Y. Kuo, and S.-T. Chen, "Synergistic effects between TiO_2 and carbon nanotubes (CNTs) in a TiO_2/CNTs system under visible light irradiation," *Environmental Technology*, vol. 34, no. 17, pp. 2513–2519, 2013.

[42] M. M. Gui, S.-P. Chai, B.-Q. Xu, and A. R. Mohamed, "Visible-light-driven MWCNT@TiO_2 core–shell nanocomposites and the roles of MWCNTs on the surface chemistry, optical properties and reactivity in CO_2 photoreduction," *RSC Advances*, vol. 4, no. 46, p. 24007, 2014.

[43] W. Zhou, K. Pan, Y. Qu et al., "Photodegradation of organic contamination in wastewaters by bonding TiO_2/single-walled carbon nanotube composites with enhanced photocatalytic activity," *Chemosphere*, vol. 81, no. 5, pp. 555–561, 2010.

[44] S. B. A. Hamid, T. L. Tan, C. W. Lai, and E. M. Samsudin, "Multiwalled carbon nanotube/TiO_2 nanocomposite as a highly active photocatalyst for photodegradation of reactive black 5 dye," *Chinese Journal of Catalysis*, vol. 35, no. 12, pp. 2014–2019, 2014.

[45] Z. Peining, A. S. Nair, Y. Shengyuan, and S. Ramakrishna, "TiO_2–MWCNT rice grain-shaped nanocomposites : synthesis, characterization and photocatalysis," *Materials Research Bulletin*, vol. 46, no. 4, pp. 588–595, 2011.

[46] D. Ramimoghadam, M. Zobir, B. Hussein, and Y. H. Taufiqyap, "The effect of sodium dodecyl sulfate (SDS) and cetyltrimethylammonium bromide (CTAB) on the properties of ZnO synthesized by hydrothermal method," *International Journal of Molecular Sciences*, vol. 13, no. 12, pp. 13275–13293, 2012.

[47] Y. Li, Y. Huo, C. Li, S. Xing, L. Liu, and G. Zou, "Thermal analysis of Cu-organic composite nanoparticles and fabrication of highly conductive copper films," *Journal of Alloys and Compounds*, vol. 649, pp. 1156–1163, 2015.

[48] R. Manivannan, A. Daniel, I. Srikanth et al., "Thermal stability of zirconia-coated multiwalled carbon nanotubes," *Defence Science Journal*, vol. 60, no. 3, pp. 337–342, 2010.